Journal of Molecular Structure 1262 (2022) 133025

Contents lists available at ScienceDirect

Journal of Molecular Structure

journal homepage: www.elsevier.com/locate/molstr

Utilization of pyrazole-perimidine hybrids bearing different substituents as corrosion inhibitors for 304 stainless steel in acidic media

Özlem UĞUZ[a], Mehmet GÜMÜŞ[b], Yusuf SERT[c], İrfan KOCA[d,*], Atıf KOCA[a,*]

[a] Department of Chemical Engineering, Faculty of Engineering, Marmara University, Istanbul 34722, Turkey
[b] Akdağmadeni Health College, Yozgat Bozok University, Yozgat 66300, Turkey
[c] Sorgun Vocational School, Yozgat Bozok University, Yozgat 66700, Turkey
[d] Department of Chemistry, Faculty of Art & Sciences, Yozgat Bozok University, Yozgat 66900, Turkey

ARTICLE INFO

Article history:
Received 15 February 2022
Revised 25 March 2022
Accepted 6 April 2022
Available online 9 April 2022

Keywords:
Pyrazole-perimidine hybrids
Corrosion inhibition
Potentiodynamic polarization
Electrochemical impedance spectroscopy
DFT

ABSTRACT

Water soluble Pyrazole-Perimidine (**PYR-PER**) hybrids bearing various anchoring groups has been synthesized and their corrosion inhibitive efficiencies for the 304 stainless steel in 1.0 M hydrochloric acid has been investigated by the electrochemical impedance spectroscopy (EIS), potentiodynamic polarization (PDP), open circuit potential (OCP) measurements, and Density Functional Theory (DFT) B3LYP functional combined with 6-311++G(d,p) basis set. The analyses show that all **PYR-PER** hybrids effectively reduced the corrosion current density, increased corrosion resistance and inhibited the corrosion of the 304 stainless steel in 1.0 M hydrochloric acid at 298 K. The results indicated that the hybrids functioned as a mixed type inhibitors with anodic suppression outweighing the cathodic one. Multi-functional heteroatoms and methyl, fluoride, chloride, and bromide substituents of pyrazole derivatives considerably enhanced the inhibition efficiencies of the hybrids. The highest corrosion inhibitive efficiency (as 97.45%) was achieved with **PYR-PER3** bearing methyl and bromide anchoring groups on the benzene group of the main **PYR-PER** structure. Some quantum chemical parameters, E_{HOMO}, E_{LUMO}, ΔE, electronegativity, chemical hardness, chemical softness, electrophilicity index, proton affinity and ΔN electron transfer were also discussed. Additionally non-linear optical properties (NLO) were investigated. The results in the B3LYP technique supported by experimental results.

1. Introduction

It is well known that metal equipment used in industry are often exposed to harsh conditions or strong cleaners such as an acidic environment. These situations cause metal equipment to corrode and weaken or eliminate their functions. For these reasons, these materials should be protected accordingly, economically, and efficiently. One of the preferred methods to protect these materials from corrosion is the use of corrosion inhibitors during the operation or cleaning of these equipment [1–4]. There are many published corrosion inhibitors in the literature for the protection of various metal specimens from acidic, salty, or similar harsh conditions [5–7]. Among the published inhibitors, numerous effective organic inhibitors which generally contain unsaturated, planar and/or aromatic structures carrying different heteroatoms, such as S, O, and N, and polar functional groups such as -OH, - OCH_3, -NH_2, -CH_3, and/or -NH, have been extensively studied as possible corrosion inhibitors [1,8–14]. Many synthetic organic compounds, such as, cinnamate [15], thiazine [16–18], imidazole [19,20], pyrazine [21], pyrrole [22], pyrazole [23], pyridine and pyrimidine [24,25], aliphatic and aromatic amines [26,27], amide [28], indole [29], quinoline [30], thiophene [31], and derivatives of the similar macrocyclic molecules were published as efficient corrosion inhibitors. Moreover, the effects of the substituents of these molecules on the corrosion rates of different metal and/or alloy samples have been investigated in ongoing papers. For instance, Liu et.al. used 5-methyl-1*H*-benzotriazole as a corrosion inhibitor for chemical mechanical polishing of bearing steel and reported that the triazole and hydrophobic methyl functional groups played important role for the protection efficiency of the inhibitor molecules [32]. In another study, Mondal investigated the corrosion inhibition efficiencies of various organic compounds, such as, imidazole, 2-methylimidazole, benzimidazole, piperazine, histidine, and an imidazoline-surfactant, any they illustrated that efficiencies

* Corresponding authors.
E-mail addresses: i_koca@yahoo.com (İ. KOCA), akoca@marmara.edu.tr (A. KOCA).

https://doi.org/10.1016/j.molstruc.2022.133025
0022-2860/

were depend on the anchoring groups and the best efficiency was obtained with the an imidazoline-surfactant inhibitor [33]. Similar studies in the literature indicated that the structures of the molecules, substituent environments, types, and positions of the substituents influenced the electronic structure, hence they had pronounced effects on the corrosion efficiency of the molecules [1,34–37].

Among the organic molecules, pyrazole with electron donating substituents were reported as one of the most preferred efficient corrosion inhibitors, and there are too many studies on the corrosion applications with its different derivatives [38–45]. For instance, Sayed et al. evaluated six pyrazole and pyrazolone derivatives as corrosion inhibitors for copper alloy dissolution. They assigned the efficiency of the molecules to the features of the heteroatoms and the unsaturated centers, which, in turn, increased their adsorption [45]. In another study, Abdallah concluded that the inhibition action of these compounds via adsorption through their active centers depended on the inductive and mesomeric effects of the substituents [46].

Dohare and coworkers reported 88–98% inhibition efficiency for three pyranpyrazole derivatives at 300 mg/L [47]. Many studies indicated that the functionality of the active pyrazolone molecules and nature of their substituent environments strongly affected the corrosion inhibitor efficiency for different metal specimens [48–53]. Similarly, pyrimidine derivatives have been investigated as another highly efficient corrosion inhibitors due to their large π-bond system with *N*-containing heterocyclic structure, which makes these molecules as strong adsorbents on metal surfaces [47,53–58]. On the other hand, there is only one reported study related to the corrosion inhibitor activity of perimidine derivatives [59], even though perimidine derivatives have larger π-bond system than the same *N*-containing heterocyclic structure of pyrimidine, which has the possibility to indicate better adsorption ability during inhibition process. He et al. reported >90% inhibition efficiencies with a concentration of < 0.15 mM 1*H*-perimidine (PER) and 1*H*-perimidin-2-amine (NPER) molecules for mild steel in acidic media [59]. These results and the functional structure of perimidine molecule show its possible usability as an efficient corrosion inhibitor.

The relationship between the molecular and electronic structures of perimidine and pyrazole inhibitors, and their corrosion inhibition potentials helps us design new corrosion inhibitors, "Pyrazole-Perimidine Hybrids (**PYR-PER**)", which contain the functionalities of both pyrazole (PYR) and perimidine (PER) heterocycles. These heterocycles are decorated with functional N=N, NH, aromatic heterocyclic groups, and electron donating by inductive effect of CH_3 substituent and by resonance effect of the polar Cl, F, and Br substituents. These functionalities have the possibility to increase electron density at the adsorption site of the inhibitor, thereby leading to achieve a better corrosion inhibitor efficiency.

To the best of our knowledge, **PYR-PER** hybrids have not been studied as corrosion inhibitors yet. Consequently, based on the expected properties of these structures, it is predicted that they may show better inhibitory activity than their counterparts in the literature. For this purpose, in this study, we have aimed to examine the corrosion inhibition performances of **PYR-PER** hybrids for 304 stainless steel in 1.0 M HCl, and to investigate the effects of Cl, F, Br and CH_3 substituents on their inhibition performance by experimental measurements and theoretical calculations. Therefore, electrochemical impedance spectroscopy (EIS), potentiodynamic polarization (PDP), open circuit potential (OCP) measurements, and theoretical calculations were performed. The effects of **PYR-PER**s as corrosion inhibitors on 304 stainless steel in an acidic environment were investigated using Density Functional Theory (DFT) B3LYP functional combined with 6-311++G(d,p) basis set.

2. Experimental

The **PYR-PER** hybrids were prepared by following the earlier described method as depicted in Fig. 1 [60]. The target compounds are obtained at the end of a four-step reaction, starting from acetophenone. Firstly, α, β-unsaturated carbonyl compounds (**2**) containing dimethylamino group were synthesized from the reactions of acetophenone derivatives with *N,N*-dimethylformamide dimethyl acetal (DMF-DMA) reagent. From the following reaction of the compound **2** with aromatic diazonium salts, the aryl hydrazonal compound (**3**) was obtained. Pyrazolyl β-ketoester derivative (**4**) was synthesized from the reaction of compound **3** with ethyl 4-chloro-3-oxobutanoate in reflux condition. In this reaction, acetone and potassium carbonate were used as the solvent and the base, respectively. In the last step, target compound (**PYR-PER**) including pyrazole and perimidine rings was obtained from the reactions of compound **4** with naphthalene-1,8-diamine.

Hydrochloric acid was purchased from Sigma-Aldrich and its solution was prepared with ultra-pure water (resistivity of 18.2 MΩ cm (at 25°C) Milli-Q, Millipore). The metal sample was a circular 304 stainless steel (304 SS) (18.18% Cr, 8.48% Ni, 1.75% Mn, 0.5% Si, 0.36% Mo, 0.051% C, 0.05% N, 0.005% S, 0.028% P and the remainder is Fe) having 1.00 cm^2 active area. The active area of the 304 SS was successively cleaned by using the previously reported method 24. The electrolytic cell was a Gamry corrosion cell, in which a three-electrode system was built. In this configuration, 304 SS, Pt wire and Ag/AgCl were used as working, counter and reference electrodes, respectively. The electrolyte was a degassed 1.0 M HCl aqueous electrolyte.

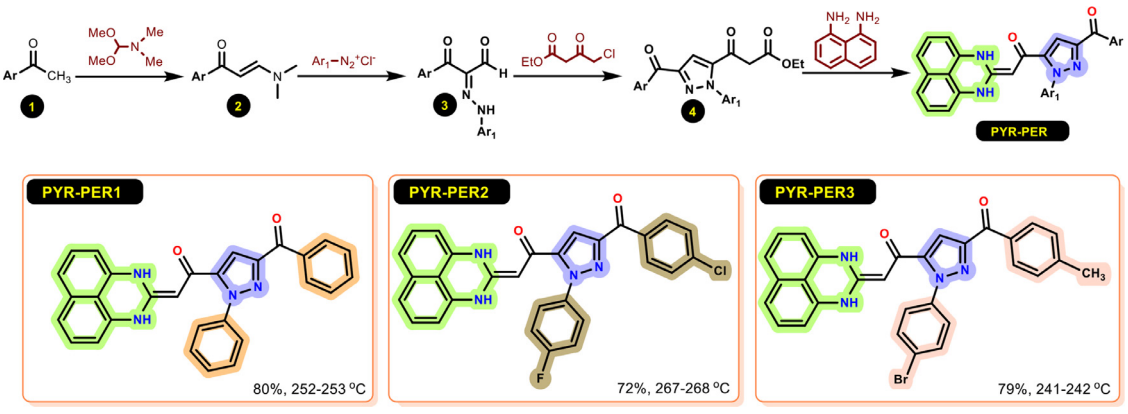

Fig. 1. Synthesis scheme and structures of **PYR-PER** hybrids.

Table 1
EIS parameters.[a]

Inhibitors	Conc.ppm (mM)	R_s(Ω cm^2)	R_p(Ω cm^2)	(χ2)x10^4	CPEY$_0$ (Ω^{-1}s^{n}cm^{-2})	n	C_{dl} (μF cm^{-2})
PYR-PER1	0	7.6	84.2	8.89	1024.00	0.87	585.00
	50 (0.15)	7.5	234.5	7.37	392.30	0.85	189.50
	150 (0.45)	6.9	376.7	2.89	267.90	0.84	115.70
	300 (0.90)	6.3	443.6	6.01	276.60	0.81	102.60
	600 (1.80)	6.2	478.2	8.46	232.00	0.85	94.31
PYR-PER2	0	7.6	84.2	8.89	1024.00	0.87	585.00
	50 (0.13)	6.6	294.3	8.43	510.90	0.84	140.50
	150 (0.40)	6.4	426.2	4.40	340.30	0.81	130.50
	300 (0.80)	6.3	496.1	8.01	329.20	0.80	115.70
	600 (1.62)	6.3	578.4	2.12	216.50	0.82	178.60
PYR-PER3	0	7.6	84.2	8.89	1024.00	0.87	585.00
	50 (0.12)	7.5	234.5	4.19	731.00	0.79	303.50
	150 (0.36)	6.9	376.7	1.26	510.90	0.84	140.50
	300 (0.72)	6.3	443.6	1.96	384.10	0.83	131.10
	600 (1.44)	6.2	478.2	8.01	329.00	0.80	126.40

[a] These parameters are derived from fitting of Nyquist plots.

Electrochemical impedance spectroscopy (EIS), potentiodynamic polarization (PDP), and open circuit potential (OCP) measurements were performed in a three-electrode system by using a Gamry Reference 300 galvanostat/potentiostat. For the corrosion test with each inhibitor, each method was performed without and then with gradual addition of the inhibitor. First of all, open circuit potential (OCP) measurements were performed after 30 min. of each addition of the inhibitor. Then, electrochemical impedance spectroscopy (EIS) analysis was carried out with an amplitude of AC signal at the frequency range of 0.01 Hz–100 kHz. Finally, potentiodynamic polarization (PDP) measurements were made within the potential range of ±0.25 V of OCP at 0.166 mV s^{-1} scan rate. Each measurement was performed three times to examine repeatability of the measurements.

Inhibitor efficiency (η%) was determined by employing Eq. (1) [61,62]:

$$\eta\% = \frac{I^{o}_{corr} - I^{inh}_{corr}}{I^{o}_{corr}} \quad (1)$$

where, I^{inh}_{corr} and I^{o}_{corr} are the corrosion current densities with and without of inhibitors, respectively.

3. Results and discussion

3.1. Electrochemical corrosion tests

The effect of the **PYR-PER** hybrids on the corrosion of 304 SS were determined by the open circuit potential (E_{ocp}), electrochemical impedance spectroscopy (EIS) and potentiodynamic polarization (PDP) measurements in 1.0 M HCl aqueous electrolyte. The determination of Eocp responses of a system versus time is generally made before any other electrochemical test since no changes in the properties of the sample occur. It is clearly seen in Fig. 2 that straight E_{ocp} vs. time curves are observed for all inhibitors due to the stabilization of E_{ocp} after a while. E_{ocp} values of all inhibitors shift towards more positive potentials with increasing inhibitor concentrations due to the adsorption of **PYR-PER** hybrids on the 304 SS surface, which obstruct the corrosion of 304 SS. Among the **PYR-PER** hybrids, **PYR-PER3** has the highest effect with more positive potential shifts on the E_{ocp} responses due to most probably strong adsorption of **PYR-PE**R3 with the help of CH_3 substituent. Due to the electron withdrawing nature by inductive effect of the Cl and F substituents on **PYR-PER2,** this molecule has less influence on the E_{ocp} responses of 304 SS.

Inhibitor abilities of **PYR-PER** hybrids were further investigated using EIS measurements. The Nyquist plots are represented in Fig. 3. All EIS parameters derived from Nyquist plots, are tabulated in Table 1. All of the recorded Nyquist plots show single capacitive arcs indicating presence of a single charge transfer process during the dissolution of 304 SS sample [42]. Nyquist plots are fitted to obtain the equivalent circuits (Fig. 3) and to evaluate basic EIS parameters, such as, the polarization resistance (R_p), constant phase element (CPE), the phase shift (n), and the goodness of the fit (χ^2). Small χ^2 values (less than 10^{-3}) show acceptability of the fitted data [63]. The obtained equivalent circuit consists of the solution

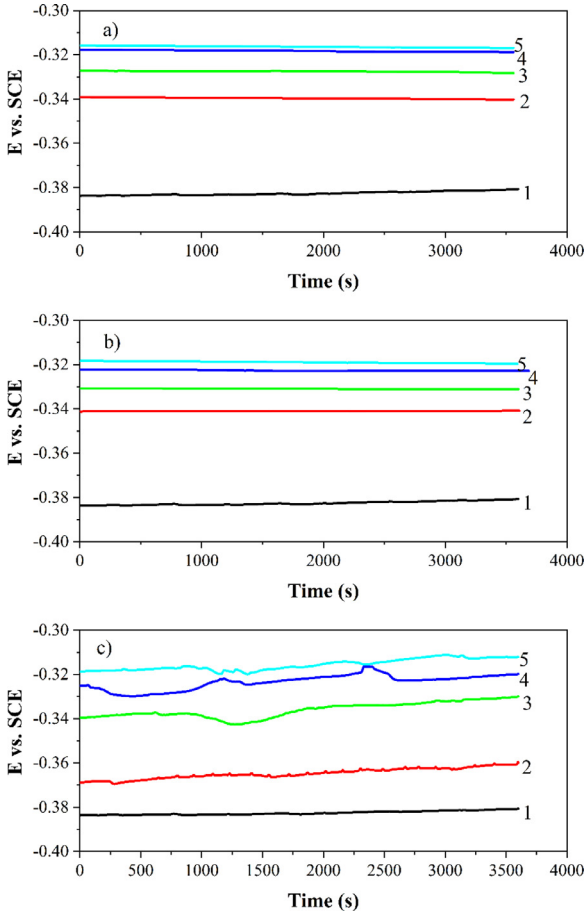

Fig. 2. E_{oc} vs. time changes of 304 SS in 1.0 M HCl solution with respect to increasing concentrations of the **PYR-PER** hybrids. (a) **PYR-PER1**, (b) **PYR-PER2**, (c) **PYR-PER3.** Concentrations: 1: blank, 2:50 ppm, 3:150 ppm, 4:300 ppm, and 5:600 ppm.

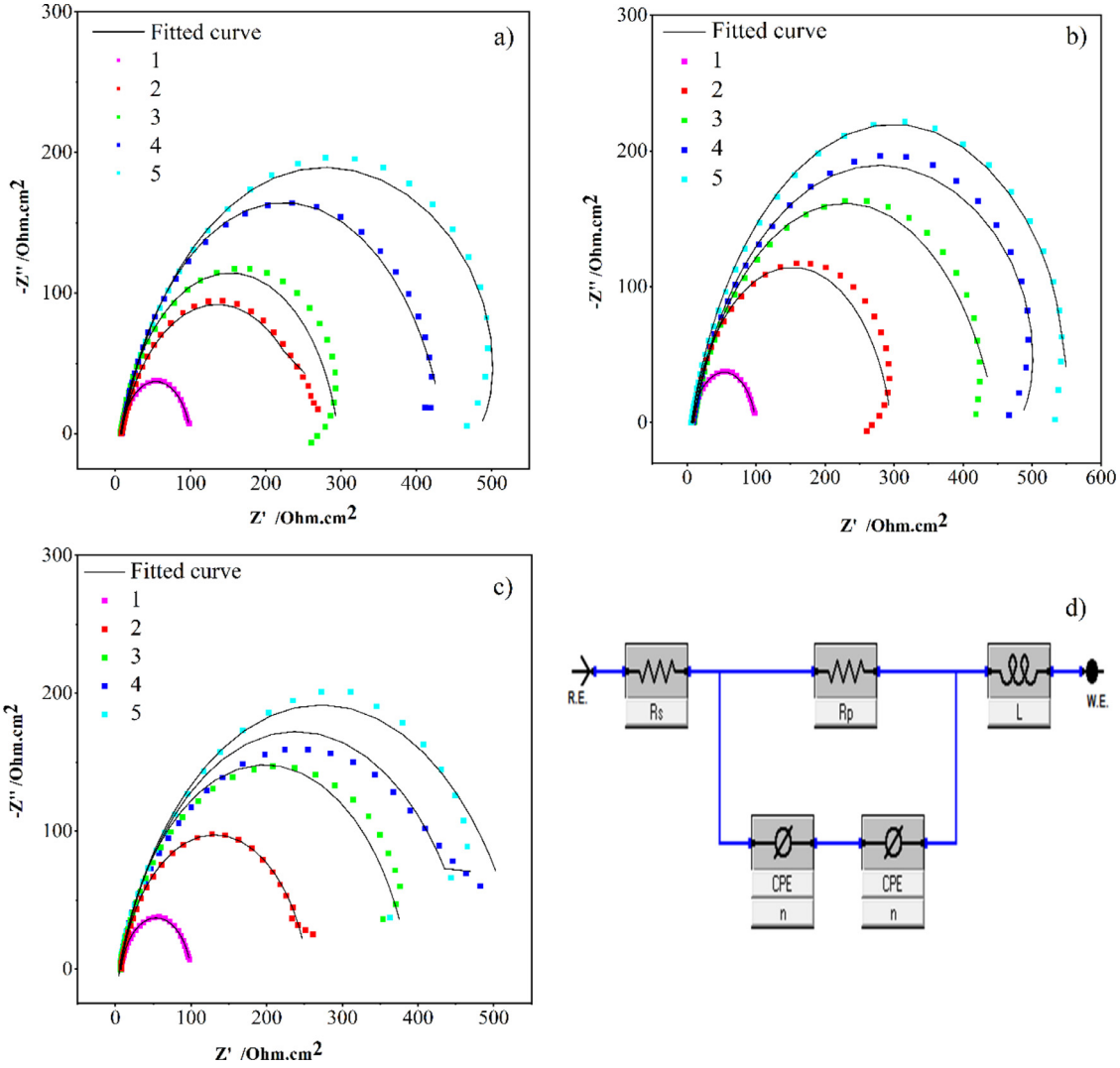

Fig. 3. EIS measurements of 304 SS in 1.0 M HCl solution containing **PYR-PER** hybrids. Nyquist graphs of (a) **PYR-PER1**, (b) **PYR-PER2**, (c) **PYR-PER3**, (d) Equivalent circuit of **PYR-PER1**. Concentrations: 1: blank, 2:50 ppm, 3:150 ppm, 4:300 ppm, and 5:600 ppm.

resistance (R_s), the polarization resistance (R_p), constant phase element (CPE), and the electric double layer capacitor (C_{dl}). The system behavior indicates that it is not an ideal capacitor, thus CPE is used instead of the capacitor. When combined in a parallel form, R_p and CPE elements are in series with the Rs element in the circuit. Inequality of Z_{re} to Z_{im} responses of the Nyquist plots addresses to the roughness of the 304 SS surface. Due to the roughness of the surface, CPE is generally used instead of the nonideal capacitors. It is clearly observed that 304 SS sample gives a curve with a small semicircle with 84.2 Ω cm^2 of R_p and 585 μF cm^{-2} of C_{dl} without inhibitors. After the addition of inhibitors, these values significantly and differently alter since the surface of the 304 SS sample changes. The diameters of the semicircles for all **PYR-PER** hybrids increase with increasing inhibitor concentrations due to the formation of adsorbed film on 304 SS surface. Thus, an increase in the polarization resistance (R_p) and a decrease in the CPE responses of the 304 SS are noted [64,65]. The Nyquist plots show that there is adsorption during corrosion process, which can be expressed by inductance (L). In the Fig. 3, inductive loops are generally observed at the positive imaginary impedance values and L values for all samples are almost comparable to each other [66]. When the curves in the Bode diagram are investigated, Bode angles shift towards higher frequencies as the impedance gets higher with respect to the addition of the inhibitor (Fig. 4). In addition, the phase angle plots get wider towards the higher frequencies as the angles increase due to the inhibitor adsorption [67–69].

As shown in Table 1, rising concentrations of all **PYR-PER** hybrids causes an increase in R_p and a decrease in CPE responses. The magnitude of these responses depends on the inhibitor activities of **PYR-PER** hybrids. Increase of R_p and decrease of CPE indicate the changes in the double layer on the 304 SS surface by replacement of the water molecules with the molecules of the inhibitors. Moreover, the decreased capacitance of the electrode also supports the adsorption of the inhibitors on the surface, limiting the 304 SS corrosion.

For further investigation of the inhibition effects of the **PYR-PER** hybrids on 304 SS, potentiodynamic polarization measurements were carried out between ±0.25 V of E_{ocp} at 0.166 mV s^{-1} scan rate in 1.0 M HCl solution at room temperature, and the results are represented in Fig. 5. The corrosion potential (E_{corr}), corrosion current (I_{corr}), and anodic and cathodic Tafel constants (β_a and β_c) are derived from these graphs and tabulated in Table 2. Accordingly, while the E_{corr} of the system shifts towards more positive potentials, I_{corr} response of the sample significantly decreases because of the increasing of the inhibitor concentrations. Moreover, the β_a values decrease gradually as the concentrations increase.

Table 2
Potentiodynamic polarization parameters.[a]

[a]Inhibitors	Conc.ppm (mM)	E_{corr}(mV)	I_{corr}(μA/cm^2)	β_a(mV/dec)	-β_c(mV/dec)	η%	Rate (mmpy)
PYR-PER1	0	-373	498	81	117	-	154.02
	50 (0.15)	-341	72	74	103	85.54	22.27
	150 (0.45)	-337	56	48	98	88.76	17.32
	300 (0.90)	-329	51	31	90	89.76	15.77
	600 (1.80)	-325	32	27	87	93.57	9.90
PYR-PER2	0	-373	498	81	117	-	154.02
	50 (0.13)	-350	193	69	112	61.24	59.69
	150 (0.40)	-343	119	51	100	76.10	36.80
	300 (0.80)	-332	63	40	92	87.35	19.48
	600 (1.62)	-327	46	38	84	90.76	14.23
PYR-PER3	0	-373	498	81	117	-	154.02
	50 (0.12)	-345	84.5	76	110	83.03	26.13
	150 (0.36)	-318	43.3	69	115	91.31	13.39
	300 (0.72)	-315	32.6	55	98	93.45	10.08
	600 (1.44)	-310	12.7	50	96	97.45	3.93

[a] All of the parameters are derived from Tafel fitting function of 'Gamry Echem Analyst' software.

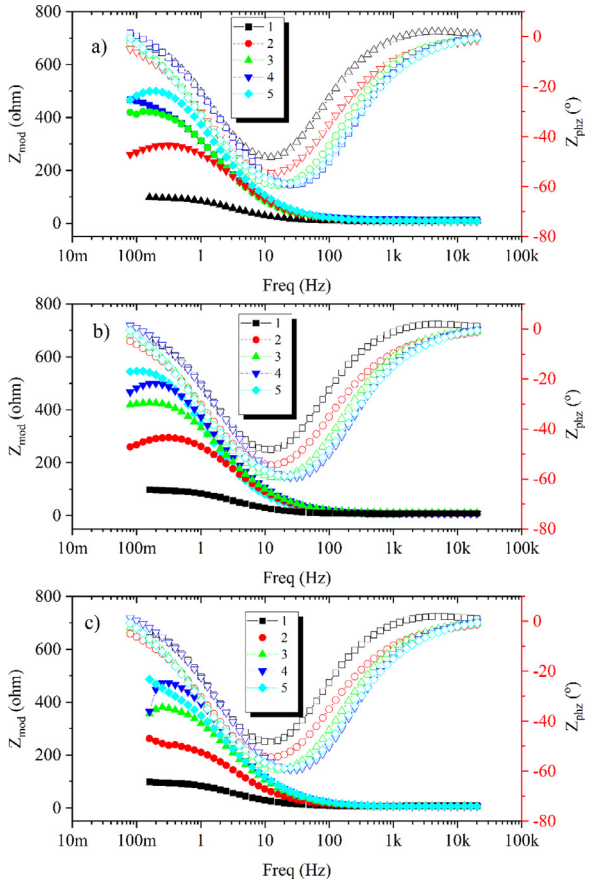

Fig. 4. Bode graphs recorded with EIS measurements of 304 SS in 1.0 M HCl solution containing **PYR-PER** hybrids. (a) **PYR-PER1**, (b) **PYR-PER2**, (c) **PYR-PER3**. Concentrations: 1: blank, 2:50 ppm, 3:150 ppm, 4:300 ppm, and 5:600 ppm.

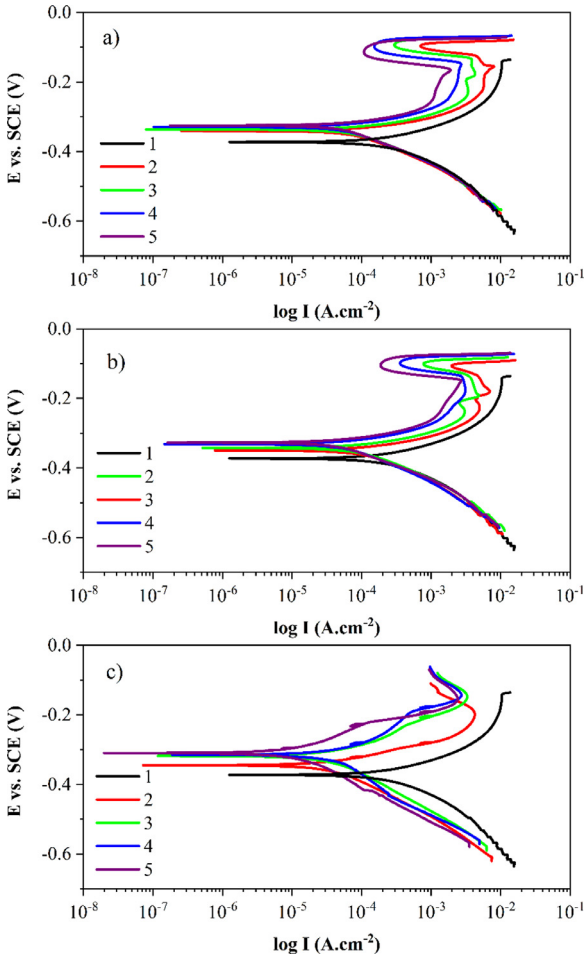

Fig. 5. Polarization resistance measurements of 304 SS in 1.0 M HCl solution with respect to increasing concentrations of the **PYR-PER** hybrids. (a) **PYR-PER1**, (b) **PYR-PER2**, (c) **PYR-PER3**. Concentrations: 1: blank, 2:50 ppm, 3:150 ppm, 4:300 ppm, and 5:600 ppm.

That indicates the passivation of the 304 SS with the adsorption of the inhibitor and hence, the hindrance of both anodic and cathodic reactions during the corrosion of the sample. All **PYR-PER** hybrids behave as mixed-type inhibitors with the dominant control of the anodic reaction.

Cathodic branches of the Tafel plot have nearly parallel responses to each other with nearly constant slope within the applied potentials. As shown in Table 2, β_c values slightly decrease as the concentrations of the inhibitors increase. This response shows that inhibition of the reduction process is resulted from the blocking of the sample surface without changing the reduction reaction mechanism. However, for the anodic branch, the nearly linear response is only observed at small overpotentials due to the inhibition of the oxidation of the metal sample with the inhibitor layer on the surface. When the potential is swept towards more positive potentials, diminishing the linearity of the curve indicates the removal of the inhibitor layer and dissolution of the met-

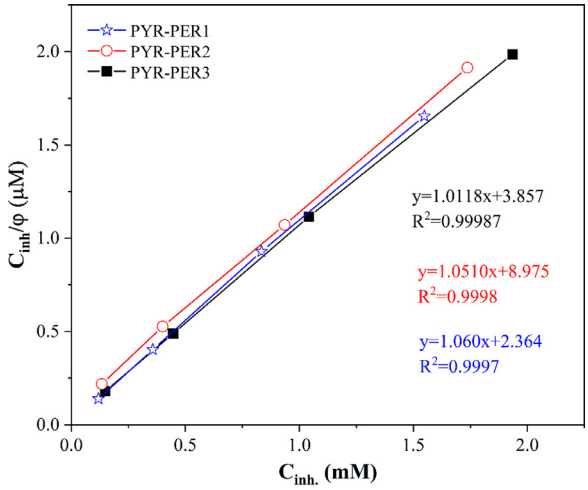

Fig. 6. Langmuir adsorption isotherms of **PYR-PER** hybrids.

als. However, the current decreases ca. between -0.25 and 0.20 V, which indicates passivation of the samples due to the formation of $\boldsymbol{Fe(Ligand)_x^{2+}}$species on the sample surface. Sharp current increases are observed at high overpotentials for the dissolution of these species and oxidation of the sample. Based on the evaluated results of the potentiodynamic polarization measurements, it can be clearly concluded that although all **PYR-PER** hybrids cause similar inhibiting features, the highest efficiency is obtained with **PYR-PER3**, which is in harmony with the EIS results. Due to the electron withdrawing nature of fluoride and chloride on **PYR-PER2**, this molecule has less efficiency than that of the unsubstituted **PYR-PER1**. With respect to data on Table 2, the order of the inhibition activities of the molecules is as **PYR-PER3**> **PYR-PER1**> **PYR-PER2**.

Corrosion inhibition process is generally resulted from the adsorption of the inhibitors on the 304 SS surface, which can be evaluated with various isotherm models. Among the possible models, the best fitting for the inhibiting behaviors of **PYR-PER** hybrids is obtained with Langmuir adsorption using the Eq. (2).

$$\frac{\boldsymbol{C}}{\boldsymbol{\theta}} = \frac{1}{\boldsymbol{K_{ads}}} + \boldsymbol{C} \tag{2}$$

where K_{ads} is the equilibrium constant of the adsorption, C is the concentration of the inhibitors, and θ is the surface coverage ratio. θ values are derived from η% values calculated from the potentiodynamic polarization data.

As shown in Fig. 6, the unity of R^2 for all isotherms indicates the agreement of the adsorption processes of **PYR-PER** hybrids on Langmuir adsorption model. K_{ads} values are found as 0.258, 0.111, and 0.149 M^{-1} for **PYR-PER1, PYR-PER2,** and **PYR-PER3**, respectively. The sign and magnitude of ΔG^0 values (derived from Eq. (3)) of the adsorption process of the inhibitors indicate spontaneous physisorption of the inhibitor molecules on the 304 SS surface. The ΔG^0 values are at the physisorption limit, so electrostatic interactions contribute to the adsorption processes for all inhibitors. $\Delta \boldsymbol{G^0_{ads}}$ values are found as -13.76, -11.68, and -14.98 kJ mol^{-1} for **PYR-PER1, PYR-PER2,** and **PYR-PER3**, respectively. K_{ads} and ΔG^0 values confirm the highest inhibition efficiency of **PYR-PER3** among the molecules.

$$\Delta \boldsymbol{G^0_{ads}} = -\boldsymbol{RTln}(1000\boldsymbol{K_{ads}} \tag{3}$$

where T is the absolute temperature, R is the gas constant in $J.mol^{-1}.K^{-1}$, and 1000 is the concentration (g L^{-1}) of water.

3.2. Quantum chemical computations and evaluations

Metal corrosion is a major issue in a variety of industrial processes, including those that employ water, alcohol, or acid. Acid solutions produce excessive corrosion in metals such as iron, copper, and aluminum. To prevent corrosion induced by acid solutions, corrosion inhibitors including nitrogen, oxygen, sulfur, and an aromatic ring are utilized. Quantum chemical computations give us a rough idea of what molecules are up to. The development of density functional theory (DFT) has tremendously aided the application of computational chemistry in the design and development of organic corrosion inhibitors. So, based on electronic/molecular characteristics and reactivity indices, DFT has allowed corrosion scientists to precisely anticipate the inhibitory efficacies of organic corrosion inhibitors [70–73]. In this part, the computations were performed with the help of Gaussian 09W package program [74] and Gauss View 5.0 [75], DFT method and B3LYP functional combined with 6-311++G(d, p) basis set. DFT investigations were carried out to better understand the nature of the interaction between the adsorption centers of Pyrazole-Perimidine Hybrids (**PYR-PER1, PYR-PER2** and **PYR-PER3**) molecules and the 304 stainless steel surface. Firstly, the optimized structures of the studied molecules in the gas and 1.0 M HCl solution phase (Polarizable Continuum Model/PCM with Integral equation formalism/IEFPCM over chk* and static (Eps) and dynamic dielectric constants for water and HCl) [76–81] were determined for theoretical corrosion evaluations and the rest of the calculations such as frontier orbitals (HOMO, LUMO and other related properties) and proton affinities were performed over these.

The highest occupied molecular orbital-HOMO and the lowest unoccupied molecular orbital-LUMO are the frontier molecular orbitals, which are directly linked to the inhibitor or activator's reactivity ability. E_{HOMO} and E_{LUMO} are employed in the DFT theorem to estimate the ionization potential (I) and electron affinity (A) given with Koopmans theorem-by Sastri and co-authors and Bondarev and et al. [82,83] and $E=|E_{HOMO}- E_{LUMO}|$ is utilized to determine the energy bandgap.

$$I = -E_{HOMO} \tag{4}$$

$$A = -E_{LUMO} \tag{5}$$

From (4) and (5) formulas, I values were calculated as 7.579, 7.586 and 7.540 eV, and E values were computed as 1.795, 1.594 and 1.760 eV within the 1M HCl for **PYR-PER1, PYR-PER2** and **PYR-PER3,** respectively. In addition to these calculated I and E, based on the theory put forward by Koopmans [84], the following values were obtained when I (X+energy → X+ + e−) and A (X +e− → X-+energy) values were calculated considering the cation and anion states of these three molecules: I ($E_{PYR\text{-}PER+}$ – $E_{PYR\text{-}PER}$) values were calculated as 8.876, 8.887 and 8.881 eV and A ($E_{PYR\text{-}PER}$ – $E_{PYR\text{-}PER\text{-}}$) values were computed as 1.709, 1.357 and 1.705 eV for **PYR-PER1, PYR-PER2** and **PYR-PER3,** respectively. As seen from the obtained scores, these values decreased compared to Tables 3–5 results. Using the highest occupied molecular orbital (E_{HOMO}) and lowest unoccupied molecular orbital (E_{LUMO}) energies [85], the chemical potential (μ) and hardness (η) values can be computed using the Koopmans theorem [82].

$$\text{Chemical Potential} = \mu = -\left(\frac{I+A}{2}\right) = \left(\frac{E_{HOMO}+E_{LUMO}}{2}\right) \tag{6}$$

$$\text{Chemical Hardness} = \eta = \left(\frac{I-A}{2}\right) = \left(\frac{E_{HOMO}-E_{LUMO}}{2}\right) \tag{7}$$

The electrophilicity index (ω) is a measurement of the energy loss produced by the maximal electron flow between acceptor and

Table 3
Parameters of **PYR-PER1** in gas/1M HCl and possible protonated points in 1M HCl.

Parameters (eV)	**PYR-PER1** in gas phase	PYR-PER1	C1(N11)	C2(N9)	C3(N3)	C4(N4)	C5(O6)	C6(O23)
E_{LUMO}	-2.091	-1.795	-1.164	-1.136	-0.494	-0.219	-0.816	-0.407
E_{HOMO}	-7.639	-7.579	-8.311	-8.393	-7.714	-7.763	-8.040	-7.633
Energy bandgap	5.548	5.784	7.147	7.257	7.220	7.544	7.223	7.227
Ionization potential	7.639	7.579	8.311	8.393	7.714	7.763	8.040	7.633
Electron affinity	2.091	1.795	1.164	1.136	0.494	0.219	0.816	0.407
Chemical hardness	2.774	2.892	3.573	3.628	3.610	3.772	3.612	3.613
Chemical softness	0.180	0.173	0.140	0.138	0.138	0.133	0.138	0.138
Electronegativity	4.865	4.687	4.738	4.764	4.104	3.991	4.428	4.020
Chemical potential	-4.865	-4.687	-4.738	-4.764	-4.104	-3.991	-4.428	-4.020
Electrophilicity index	4.266	3.798	3.141	3.128	2.332	2.111	2.714	2.236
Planarity (best structural geometry)	C1	C1	C1	C1	C1	C1	C1	C1

Table 4
Parameters of **PYR-PER2** in gas/1M HCl and possible protonated points in 1M HCl.

Parameters (eV)	**PYR-PER2** in gas phase	PYR-PER2	C1(N11)	C2(N9)	C3(N3)	C4(N4)	C5(O6)	C6(O23)	C7(Cl37)	C8(F36)
E_{LUMO}	-1.677	-1.594	-1.122	-1.138	-0.350	-0.116	-0.764	-0.567	-1.045	-1.341
E_{HOMO}	-7.784	-7.586	-8.317	-8.352	-7.725	-7.775	-8.049	-7.640	-7.607	-7.622
Energy bandgap	6.107	5.992	7.196	7.214	7.374	7.660	7.286	7.073	6.562	6.281
Ionization potential	7.784	7.586	8.317	8.352	7.725	7.775	8.049	7.640	7.607	7.622
Electron affinity	1.677	1.594	1.122	1.138	0.350	0.116	0.764	0.567	1.045	1.341
Chemical hardness	3.054	2.996	3.598	3.607	3.687	3.830	3.643	3.537	3.281	3.140
Chemical softness	0.164	0.167	0.139	0.139	0.136	0.131	0.137	0.141	0.152	0.159
Electronegativity	4.730	4.590	4.720	4.745	4.038	3.946	4.406	4.103	4.326	4.481
Chemical potential	-4.730	-4.590	-4.720	-4.745	-4.038	-3.946	-4.406	-4.103	-4.326	-4.481
Electrophilicity index	3.664	3.516	3.096	3.121	2.211	2.032	2.665	2.381	2.852	3.198
Planarity (best structural geometry)	C1	C1	C1	C1	C1	C1	C1	C1	C1	C1

Table 5
Parameters of **PYR-PER3** in gas/1M HCl and possible protonated points in 1M HCl.

Parameters (eV)	**PYR-PER3** in gas phase	PYR-PER3	C1(N11)	C2(N9)	C3(N3)	C4(N4)	C5(O6)	C6(O23)	C7(Br36)
E_{LUMO}	-2.020	-1.760	-1.094	-1.134	-0.469	-0.198	-0.823	-0.407	-1.358
E_{HOMO}	-7.700	-7.540	-8.321	-8.351	-7.718	-7.769	-8.053	-7.635	-7.616
Energy bandgap	5.680	5.781	7.226	7.216	7.249	7.571	7.230	7.228	6.258
Ionization potential	7.700	7.540	8.321	8.351	7.718	7.769	8.053	7.635	7.616
Electron affinity	2.020	1.760	1.094	1.134	0.469	0.198	0.823	0.407	1.358
Chemical hardness	2.840	2.890	3.613	3.608	3.625	3.785	3.615	3.614	3.129
Chemical softness	0.176	0.173	0.138	0.139	0.138	0.132	0.138	0.138	0.160
Electronegativity	4.860	4.650	4.708	4.743	4.094	3.983	4.438	4.021	4.487
Chemical potential	-4.860	-4.650	-4.708	-4.743	-4.094	-3.983	-4.438	-4.021	-4.487
Electrophilicity index	4.158	3.741	3.067	3.117	2.312	2.096	2.724	2.237	3.218
Planarity (best structural geometry)	C1	C1	C1	C1	C1	C1	C1	C1	C1

donor. It is computed as follows:

$$\text{Electrophilicity index} = \omega = \frac{\mu^2}{2\eta} \tag{8}$$

As seen in Eq. (9), the negative of the chemical potential is expressed as electronegativity (χ):

$$\text{Electronegativity} = \chi = \left(\frac{I + A}{2}\right) = -\left(\frac{E_{HOMO} + E_{LUMO}}{2}\right) \tag{9}$$

Chemical softness is the inverse of hardness and is calculated as:

$$\textit{Chemical softness} = \xi = \frac{1}{2\eta} = \frac{1}{(E_{HOMO} - E_{LUMO})} \tag{10}$$

Firstly, the order of **PYR-PER** Hybrids was obtained from their calculations in the gas phase according to HOMO-LUMO gap, and electronegativity values, which were calculated with DFT/B3LYP combined with 6-311++G(d,p) taking into account the above equations: $\Delta E_{PYR\text{-}PER1} < \Delta E_{PYR\text{-}PER3} < \Delta E_{PYR\text{-}PER2}$ and $\chi_{PYR\text{-}PER1} < \chi_{PYR\text{-}PER3} < \chi_{PYR\text{-}PER2}$. Additionally, all parameters related to frontier molecular orbital energies were computed and given in the first columns of Tables 3–5 and HOMO-LUMO electron distributions were given in Fig. 7. Considering these results, the functional groups and their symmetries (calculations were performed without any symmetry restrictions for the title compounds C1: identity operation), it is decided to apply the same experimental circumstances for the molecules (**PYR-PER1, PYR-PER2** and **PYR-PER3**), and to calculate the frontier orbitals in 1M HCl in water solvation system over the checkpoint files. Here, the solvent's influence has been taken into account in the computational computations. Additionally, the connections between the frontier orbital energies and the relevant parameters and the candidates that could be corrosion inhibitors there are some conditions to be met: E_{HOMO} is often associated with the electron donating ability of the molecule. Therefore, inhibitors with high E_{HOMO} values tend to donate their electrons to a suitable acceptor with a low vacant molecular orbital energy. In contrast, E_{LUMO} indicates the electron accepting ability of the molecule, the lower its value, the higher its ability to accept electrons [86]. Later, the HOMO-LUMO gap energy difference is another important factor in defining molecular activity. Thus, when ΔE decreases, inhibitory activity increases [87–89]. On the other hand, other quantum chemical parameters given in Tables 3–5 are very useful for elucidating the chemical reactivity of molecules and provide important clues for theoretically predicting the inhibition efficiency of molecules [90–92]. Namely, chemical softness (ξ) is a measure of the polarizability of chemical species. Soft molecules easily donate their electrons to the metal surface

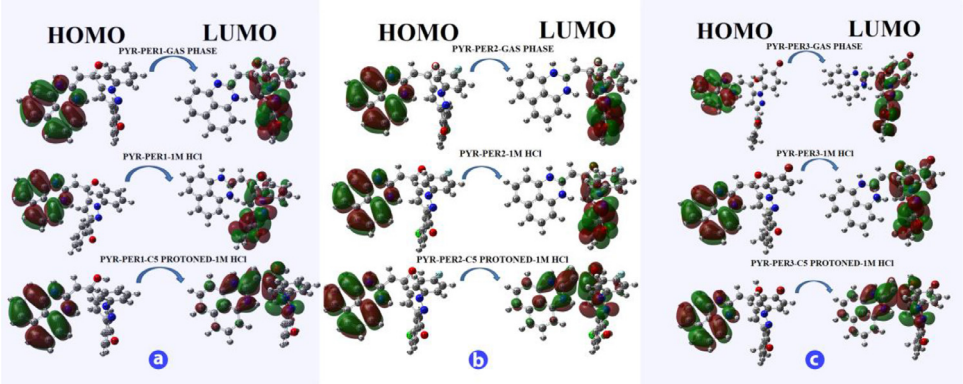

Fig. 7. HOMO and LUMO distributions of neutral and protonated forms of **PYR-PER** molecules.

and are described as good corrosion inhibitors [93]. According to the results, when a metal and an inhibitor approach each other, electrons flow from an inhibitor with a low electronegativity value to a metal with a high electronegativity value until their chemical potentials or electronegativities are equal [93]. In general, a low electronegativity inhibitor molecule is associated with high electron donating affinity and therefore exhibits higher inhibition efficiency compared to an inhibitor with higher electronegativity. To summarize these criteria for an inhibitor candidate:

- E_{HOMO} should be high,
- E_{LUMO} should be low,
- ΔE should be low,
- Chemical softness (ξ) should be high and Chemical hardness (η) should be low,
- Electronegativity should be low.

When the obtained results are compared with alternative new inhibitors suggested in the literature [91,94] in terms of HOMO, LUMO and energy bandgap (ΔE), namely for novel gossypol–indole modification (GIM) [94], these parameters were reported as -1.32, -5.01 and 3.69 eV, respectively; again for benzyl azide (BA) and butyn-1-ol (BOL) [91] were calculated as -7.06, -1.21, 5.85 and -7.54, -0.47 and 7.07 eV, respectively. The founded results for our molecules look very promising as a new inhibitor. In our system, considering the calculations in 1M HCl in water solvation system, the parameters were calculated with DFT/B3LYP, 6-311++G(d,p) and given in the second columns of Tables 3–5. Also, the HOMO-LUMO distributions in salvation system were depicted in Fig. 7. As demonstrated in Fig. 7, the HOMO-LUMO distributions have almost the same distributions both in the gas phase and in the mixture phase. In other words, HOMO-LUMO distributions are not affected by the phase difference. To sum up, this comparison can be made between these parameters: $E_{HOMO\ PYR\text{-}PER3} > E_{HOMO\ PYR\text{-}PER1} > E_{HOMO\ PYR\text{-}PER2}$; $E_{LUMO\ PYR\text{-}PER2} > E_{LUMO\ PYR\text{-}PER3} > E_{LUMO\ PYR\text{-}PER1}$; $\Delta E_{\ PYR\text{-}PER2} > \Delta E_{\ PYR\text{-}PER1} > \Delta E_{\ PYR\text{-}PER3}$; $\xi_{\ PYR\text{-}PER1} = \xi_{\ PYR\text{-}PER3} > \xi_{\ PYR\text{-}PER1}$; $\eta_{\ PYR\text{-}PER2} > \eta_{\ PYR\text{-}PER1} > \eta_{\ PYR\text{-}PER3}$ and $\chi_{\ PYR\text{-}PER1} > \chi_{\ PYR\text{-}PER3} > \chi_{\ PYR\text{-}PER2}$. Although the parameters such as E_{HOMO}, E_{LUMO}, ΔE, chemical softness, chemical hardness, and electronegativity verify the usability of the considered molecules as corrosion inhibitors, proton affinity and ΔN values should also be checked.

Proton affinity determines the ability of an atom or a molecule to accept protons in a gas phase. Proton affinity energy (PA), defined as the protonation of the molecule in the gas phase, is used as an important parameter when studying systems involving proton transfer reactions [90]. PA is also an important parameter used to predict the inhibition efficiency of chemical compounds [95]. The most important point to note here is that a chemical compound with high proton affinity acts as a good corrosion inhibitor. The protonation points were previously determined for Pyrazole-Perimidine Hybrids (**PYR-PER1, PYR-PER2** and **PYR-PER3**), and the PA values were computed with DFT method, B3LYP functional combined with 6-311++G(d, p) basis set. The HOMO, LUMO energies, HOMO-LUMO gap values and other related parameters for protonated forms were obtained and are given in Tables 3–5.

The obtained PA values are shown in Fig. 8. The highest PA values for **PYR-PER1, PYR-PER2** and **PYR-PER3** molecules are observed on O6 atoms (according to their optimized numbering format) and their PA values were found as 272.862, 272.648 and 273.860 KJ mol^{-1}, respectively (**PYR-PER3>PYR-PER1>PYR-PER2**). It is observed that the obtained results by considering the PA values are quite consistent with the experimentally obtained results.

Finally, ΔN values of inhibitor molecules in both neutral and protonated forms are determined. The value of electrons transmitted from a corrosion inhibitor molecule is calculated using Sanderson's electronegativity equalization [96,97]:

$$\Delta N = \frac{\chi_M - \chi_{inh}}{2(\eta_M - \eta_{inh})} \tag{11}$$

where χ_M and η_M are the electronegativity and chemical hardness of metal (for 304 stainless steel about $\chi_M = 7eV$ and $\eta_M = 0eV$), χ_{inh} and η_{inh} are the electronegativity and chemical hardness of inhibitor Pyrazole-Perimidine Hybrids (**PYR-PER1, PYR-PER2** and **PYR-PER3**). The calculated ΔN values for the neutral **PYR-PER1, PYR-PER2** and **PYR-PER3** were 0.400, 0.402 and 0.407, respectively and for the protonated **PYR-PER1, PYR-PER2** and **PYR-PER3,** ΔN values were calculated as 0.383, 0.356 and 0.354, respectively. If $\Delta N > 0$, electron transport from the inhibitor molecule to the metal surface is said to occur. When the inhibitor molecule's electron-donating ability at the metal surface is less than 0.36, the greatest inhibition efficiencies are achieved according to the literature [90,96–100]. According to the situation in this study, the ΔN values show that **PYR-PER3** has a strong ability to donate electrons to iron atoms, allowing them to connect with the metal surface via coordination bonds, providing an effective protective layer that prevents metal corrosion. The protonated forms of the molecules have lower electronegativity and greater chemical hardness than neutral forms; these suggest that in an acidic media, the protonated parts of the **PYR-PER1, PYR-PER2** and **PYR-PER3** molecules have a beneficial effect on corrosion inhibition [101–103]. Additionally, the HOMO and LUMO distributions of **PYR-PER1, PYR-PER2** and **PYR-PER3** molecules for the neutral forms in gas phase, neutral and protonated forms in 1M HCl solution phase are depicted in Fig. 7. As stated above, the HOMO-LUMO distributions have almost the same distributions both in the gas phase and in the mixture phase for neutral forms. Besides, the LUMO distributions shift onto the pyrimidine moiety for the protonated forms in all three molecules. All the quantum chemical computations give

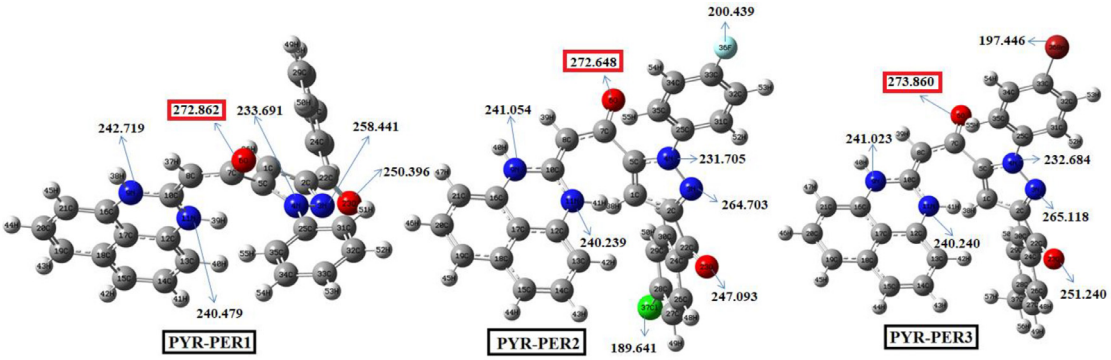

Fig. 8. Proton affinity values of optimized **PYR-PERs** molecules.

the corrosion inhibitor order as **PYR-PER3>PYR-PER1>PYR-PER2** in DFT/B3LYP method/functional combined with 6-311++G(d,p) basis set.

3.3. Non-linear optical (NLO) properties

Because of their various applications in medicine, molecular switches, luminescent materials, laser technology, spectroscopic and electrochemical sensors, data storage, microfabrication and imaging, modulation of optical signals, and telecommunication, nonlinear optical (NLO) materials have played a significant role in recent decades. The fact that organic materials have strong NLO characteristics distinguishes them [104,105]. Based on this mentioned literature, NLO parameters such as mean polarizability (α_{total}), anisotropy of polarizability ($\Delta\alpha$), first order hyper polarizability (β_0) and dipole moments of **PYR-PER1, PYR-PER2** and **PYR-PER3** compounds were computed with DFT-B3LYP/6-311++G(d,p) in 1.0 M HCl solution phase in this part. To compute these parameters, the benefited equations for our molecules are:

$$\alpha_{total} = \frac{1}{3}(\alpha_{xx} + \alpha_{yy} + \alpha_{zz}) \tag{1a}$$

$$\Delta\alpha = \frac{1}{\sqrt{2}}\left[(\alpha_{xx} - \alpha_{yy})^2 + (\alpha_{yy} - \alpha_{zz})^2 + (\alpha_{zz} - \alpha_{xx})^2 + 6a_{xz}^2 + 6a_{xy}^2 + 6a_{yz}^2\right]^{1/2} \tag{2a}$$

$$\beta_0 = \left[(\beta_{xxx} + \beta_{xyy} + \beta_{xzz})^2 + (\beta_{yyy} + \beta_{yzz} + \beta_{yxx})^2 + (\beta_{zzz} + \beta_{zxx} + \beta_{zyy})^2\right]^{1/2} \tag{3a}$$

$$\mu_{total} = \left(\mu_x^2 + \mu_y^2 + \mu_z^2\right)^{1/2} \tag{4a}$$

All computed NLO values were given in Table 6, and from this table we can say that the order of the mean polarizability (α_{total}) is **PYR-PER3** α_{total}> **PYR-PER2** α_{total}> **PYR-PER1** α_{total}, secondly, the order of anisotropy of polarizability ($\Delta\alpha$): **PYR-PER3** $\Delta\alpha$> **PYR-PER1** $\Delta\alpha$> **PYR-PER2** $\Delta\alpha$, and thirdly the order of the first order hyper polarizabilities (β_0) is **PYR-PER2** β_0> **PYR-PER3** β_0> **PYR-PER1** β_0. From the Table 6, the order of the dipole moment magnitudes is as follows: **PYR-PER3** μ_{total} > **PYR-PER1** μ_{total} > **PYR-PER2** μ_{total}. As can be seen from the NLO results, the polarization tendencies are dominant as **PYR-PER3>PYR-PER1>PYR-PER2**, and this is also seen in the inhibition performance.

Table 6
The electric dipole moment, polarizability, and first order hyperpolarizability values of the title compound.

PYR-PER1			
Parameters	Value (esu)	Parameters	Value (esu)
α_{xx}	6.31891214E-23	β_{xxx}	3.7847748489E-30
α_{xy}	-7.57330324E-24	β_{xyy}	-1.1208672088E-30
α_{xz}	-2.08587794E-24	β_{xzz}	-5.6088306959E-30
α_{yy}	5.42455056E-23	β_{yyy}	-2.6736231170E-31
α_{yz}	8.95023876E-24	β_{yxx}	4.0222104561E-30
α_{zz}	5.15425770E-23	β_{yzz}	8.2255768820E-32
α_{total}	56.3257347E-24	β_{zzz}	1.2528945214E-30
$\Delta\alpha$	23.1712276E-24	β_{zxx}	-9.9030826234E-30
μ_x	-3.3206032	β_{zyy}	-3.5496216480E-30
μ_y	0.6135639	β_0	131.23692170E-31
μ_z	0.7235704		
μ_{total}	3.4534650		
PYR-PER2			
Parameters	Value (esu)	Parameters	Value (esu)
α_{xx}	6.04862365E-23	β_{xxx}	-7.7442882781E-31
α_{xy}	-9.93160418E-24	β_{xyy}	9.5178646977E-31
α_{xz}	6.93102427E-24	β_{xzz}	1.8169379260E-30
α_{yy}	5.88979986E-23	β_{yyy}	5.4692607327E-30
α_{yz}	3.27035164E-24	β_{yxx}	-2.0641556942E-30
α_{zz}	5.44815266E-23	β_{yzz}	-5.7190728844E-30
α_{total}	57.9552539E-24	β_{zzz}	-1.0295192704E-30
$\Delta\alpha$	22.3864984E-24	β_{zxx}	6.1673339014E-30
μ_x	-3.2902345	β_{zyy}	8.5409575133E-30
μ_y	-0.2508788	β_0	140.15722221E-31
μ_z	3.5127163		
μ_{total}	1.2044054		
PYR-PER3			
Parameters	Value (esu)	Parameters	Value (esu)
α_{xx}	7.31896640E-23	β_{xxx}	1.2827389089E-30
α_{xy}	5.75726232E-24	β_{xyy}	-2.2511086654E-30
α_{xz}	-5.74049938E-24	β_{xzz}	4.5583328232E-30
α_{yy}	5.48192825E-23	β_{yyy}	-5.5143647435E-30
α_{yz}	6.23416697E-24	β_{yxx}	1.5901810517E-30
α_{zz}	5.57701484E-23	β_{yzz}	4.9036348381E-30
α_{total}	61.2596983E-24	β_{zzz}	1.3149952396E-30
$\Delta\alpha$	25.2150751E-24	β_{zxx}	-9.7709809774E-30
μ_x	3.6830726	β_{zyy}	-4.9520261017E-30
μ_y	1.9490667	β_0	139.14810127E-31
μ_z	0.7515011		
μ_{total}	4.2342223		

4. Conclusions

In summary, Pyrazole-Perimidine Hybrids successively inhibit the corrosion of the 304 stainless steel in 1.0 M hydrochloric acid. The electrochemical impedance spectroscopy (EIS), potentiodynamic polarization (PDP), and open circuit potential (OCP) measurements clearly indicate the influences of unsaturated, planar and/or aromatic structures carrying -N-N and -NH functional groups on Pyrazole-Perimidine derivatives on the inhibitor effi-

ciency. Moreover, different electron releasing/withdrawing characteristics of the substituents on these molecules alter their corrosion inhibition efficiencies. The expected inhibition performances are associated with the frontier orbital energies and other related parameters. Although it is decided by looking at the parameters such as E_{HOMO}, E_{LUMO}, ΔE, chemical softness, chemical hardness, electronegativity of the considered molecules as corrosion inhibitors, proton affinity and ΔN values should also be checked. According to both proton affinity (PA) and fraction of electron transferred (ΔN) values, the order of inhibition performances was obtained as **PYR-PER3**>**PYR-PER1**>**PYR-PER2**, which is consistent with the experimental results. Additionally, these scores were supported by NLO analysis in terms of polarization tendencies. All computations were performed in both gas (neutral form) and liquid phase (neutral and protonated forms). These compounds are highly significant in the rational design of novel Pyrazole-Perimidine Hybrids as corrosion inhibitors, as shown in tables. Overall, **PYR-PER3** demonstrated a high inhibitory efficiency for 304 stainless steel corrosion in 1M HCl. All in all, the current research offers a theoretical insight to study the molecular corrosion inhibitors which improve corrosion inhibition performances.

Authors' statement

Özlem UĞUZ: Conducting the research and investigation process, specifically performing the experiments and data/evidence collection; Preparation of the published work.

Mehmet GÜMÜŞ: Application of the computational techniques to analyze data; Preparation of the published work.

Yusuf SERT: Conducting the research and investigation process, specifically performing the experiments and data/evidence collection. Application of the computational techniques to analyze data.

İrfan KOCA: Ideas; formulation or evolution of overarching research goals and aims; Development and design of methodology, Acquisition of the financial support for the project leading to this publication.

Atıf KOCA: Preparation, creation and/or presentation of the published work by those from the original research group, specifically critical review, commentary or revision including pre-or postpublication stages.

Declaration of Competing Interest

The authors declare that they have no known competing financial interests or personal relationships that could have appeared to influence the work reported in this paper.

Acknowledgments

This work was supported by the Science and Technology Practice & Research Centre of Yozgat Bozok University [Grant Number: 6602b-FEF/16-9]. Atıf KOCA thanks to Turkish Academy of Scientists (TÜBA) for the financial support. The authors especially thank to Prof. Dr. Fatih UCUN for offering access to software used in the theoretical studies.

References

[1] C. Verma, L. Olasunkanmi, E.E. Ebenso, M. Quraishi, Substituents effect on corrosion inhibition performance of organic compounds in aggressive ionic solutions: a review, J. Mol. Liq. 251 (2018) 100–118.
[2] D. Quy Huong, T. Duong, P.C. Nam, Effect of the structure and temperature on corrosion inhibition of thiourea derivatives in 1.0 M HCl solution, ACS Omega 4 (11) (2019) 14478–14489.
[3] V.S. Sastri, J.R. Perumareddi, M. Elboujdaini, Selection of corrosion inhibitors, Corros. Eng. Sci. Technol. 40 (3) (2005) 270–272.
[4] H. Ju, X. Li, N. Cao, F.F. Wang, Y.F. Liu, Y. Li, Schiff-base derivatives as corrosion inhibitors for carbon steel materials in acid media: quantum chemical calculations, Corros. Eng. Sci. Technol. 53 (1) (2018) 36–43.
[5] W.Q. Chen, B.L. Nie, M. Liu, H.J. Li, D.Y. Wang, W.W. Zhang, Y.C. Wu, Mitigation effect of quinazolin-4(3H)-one derivatives on the corrosion behaviour of mild steel in HCl, Colloids Surf. A 627 (2021) 127188..
[6] V. Saraswat, M. Yadav, Improved corrosion resistant performance of mild steel under acid environment by novel carbon dots as green corrosion inhibitor, Colloids Surf. A 627 (2021) 127172.
[7] M.M. Solomon, I.B. Onyeachu, D.I. Njoku, S.C. Nwanonenyi, E.E. Oguzie, Adsorption and corrosion inhibition characteristics of 2-(chloromethyl) benzimidazole for C1018 carbon steel in a typical sweet corrosion environment: effect of chloride ion concentration and temperature, Colloids Surf. A 610 (2021) 125638.
[8] R.K. Gupta, M. Malviya, C. Verma, M. Quraishi, Aminoazobenzene and diaminoazobenzene functionalized graphene oxides as novel class of corrosion inhibitors for mild steel: experimental and DFT studies, Mater. Chem. Phys. 198 (2017) 360–373.
[9] R.K. Gupta, M. Malviya, C. Verma, N.K. Gupta, M. Quraishi, Pyridine-based functionalized graphene oxides as a new class of corrosion inhibitors for mild steel: an experimental and DFT approach, RSC Adv. 7 (62) (2017) 39063–39074.
[10] C. Verma, E.E. Ebenso, M. Quraishi, Ionic liquids as green and sustainable corrosion inhibitors for metals and alloys: an overview, J. Mol. Liq. 233 (2017) 403–414.
[11] M. Khan, A. Mahmood, H.Z. Alkhathlan, Characterization of leaves and flowers volatile constituents of Lantana camara growing in central region of Saudi Arabia, Arab. J. Chem. 9 (6) (2016) 764–774.
[12] F. Atmani, D. Lahem, M. Poelman, C. Buess-Herman, M.G. Olivier, Mild steel corrosion in chloride environment: effect of surface preparation and influence of inorganic inhibitors, Corros. Eng. Sci. Technol. 48 (1) (2013) 9–18.
[13] M. Forsyth, M. Seter, M.Y. Tan, B. Hinton, Recent developments in corrosion inhibitors based on rare earth metal compounds, Corros. Eng. Sci. Technol. 49 (2) (2014) 130–135.
[14] I. Milosev, A. Kokalj, M. Poberznik, C. Carriere, D. Zimerl, J. Iskra, A. Nemes, D. Szabo, S. Zanna, A. Seyeux, D. Costa, J. Rabai, P. Marcus, The effects of perfluoroalkyl and alkyl backbone chains, spacers, and anchor groups on the performance of organic compounds as corrosion inhibitors for aluminum investigated using an integrative experimental-modeling approach, J. Electrochem. Soc. 168 (7) (2021) 071506.
[15] M. Forsyth, M. Seter, M. Tan, B. Hinton, Recent developments in corrosion inhibitors based on rare earth metal compounds, Corros. Eng. Sci. Technol. 49 (2) (2014) 130–135.
[16] M. Quraishi, R. Sardar, Aromatic triazoles as corrosion inhibitors for mild steel in acidic environments, Corrosion 58 (09) (2002) NACE–02090748.
[17] A.B. Tadros, B. Abd-el-Nabey, Inhibition of the acid corrosion of steel by 4-amino-3-hydrazino-5-thio-1, 2, 4-triazoles, J. Electroanal. Chem. Interfac. Electrochem. 246 (2) (1988) 433–439.
[18] M. ElBelghiti, Y. Karzazi, A. Dafali, B. Hammouti, F. Bentiss, I. Obot, I. Bahadur, E.-E. Ebenso, Experimental, quantum chemical and Monte Carlo simulation studies of 3, 5-disubstituted-4-amino-1, 2, 4-triazoles as corrosion inhibitors on mild steel in acidic medium, J. Mol. Liq. 218 (2016) 281–293.
[19] I. Obot, S. Umoren, Z. Gasem, R. Suleiman, B. El Ali, Theoretical prediction and electrochemical evaluation of vinylimidazole and allylimidazole as corrosion inhibitors for mild steel in 1 M HCl, J. Ind. Eng. Chem. 21 (2015) 1328–1339.
[20] K. Zhang, B. Xu, W. Yang, X. Yin, Y. Liu, Y. Chen, Halogen-substituted imidazoline derivatives as corrosion inhibitors for mild steel in hydrochloric acid solution, Corros. Sci. 90 (2015) 284–295.
[21] K. Tebbji, B. Hammouti, H. Oudda, A. Ramdani, M. Benkadour, The inhibitive effect of bipyrazolic derivatives on the corrosion of steel in hydrochloric acid solution, Appl. Surf. Sci. 252 (5) (2005) 1378–1385.
[22] C. Verma, E. Ebenso, I. Bahadur, I. Obot, M. Quraishi, 5-(Phenylthio)-3H-pyrrole-4-carbonitriles as effective corrosion inhibitors for mild steel in 1 M HCl: experimental and theoretical investigation, J. Mol. Liq. 212 (2015) 209–218.
[23] G.H. Sayed, M.E. Azab, K.E. Anwer, M.A. Raouf, N.A. Negm, Pyrazole, pyrazolone and enaminonitrile pyrazole derivatives: synthesis, characterization and potential in corrosion inhibition and antimicrobial applications, J. Mol. Liq. 252 (2018) 329–338.
[24] S. Abd El-Maksoud, A. Fouda, Some pyridine derivatives as corrosion inhibitors for carbon steel in acidic medium, Mater. Chem. Phys. 93 (1) (2005) 84–90.
[25] C. Verma, K.Y. Rhee, M. Quraishi, E.E. Ebenso, Pyridine based N-heterocyclic compounds as aqueous phase corrosion inhibitors: a review, J. Taiwan Inst. Chem. Eng. 117 (2020) 265–277.
[26] R. Rihan, R. Shawabkeh, N. Al-Bakr, The effect of two amine-based corrosion inhibitors in improving the corrosion resistance of carbon steel in sea water, J. Mater. Eng. Perform. 23 (3) (2014) 693–699.
[27] K. Khaled, K. Babić-Samardžija, N. Hackerman, Theoretical study of the structural effects of polymethylene amines on corrosion inhibition of iron in acid solutions, Electrochim. Acta 50 (12) (2005) 2515–2520.
[28] D.S. Chauhan, M.A. Quraishi, M.A.J. Mazumder, S.A. Ali, N.A. Aljeaban, B.G. Alharbi, Design and synthesis of a novel corrosion inhibitor embedded with quaternary ammonium, amide and amine motifs for protection of carbon steel in 1 M HCl, J. Mol. Liq. 317 (2020) 113917.
[29] G. Avci, Corrosion inhibition of indole-3-acetic acid on mild steel in 0.5 M HCl, Colloids Surf. A 317 (1-3) (2008) 730–736.
[30] C. Verma, M. Quraishi, E.E. Ebenso, Quinoline and its derivatives as corrosion inhibitors: a review, Surf. Interfaces 21 (2020) 100634.

[31] S. Issaadi, T. Douadi, A. Zouaoui, S. Chafaa, M.A. Khan, G. Bouet, Novel thiophene symmetrical Schiff base compounds as corrosion inhibitor for mild steel in acidic media, Corros. Sci. 53 (4) (2011) 1484–1488.
[32] J.W. Liu, L. Jiang, H.Q. Wu, T. Zhao, L.M. Qian, 5-Methyl-1H-benzotriazole as an effective corrosion inhibitor for ultra-precision chemical mechanical polishing of bearing steel, J. Electrochem. Soc. 167 (13) (2020) 131502.
[33] S.K. Mondal, S.R. Taylor, The identification and characterization of organic corrosion inhibitors: correlation of a computational model with experimental results, J. Electrochem. Soc. 161 (10) (2014) C476–C485.
[34] G. Avci, Corrosion inhibition of indole-3-acetic acid on mild steel in 0.5 M HCl, Colloids Surf. A 317 (1-3) (2008) 730–736.
[35] M. Galai, M. Rbaa, H. Serrar, M. Ouakki, A. Ech-chebab, A.S. Abousalem, E. Ech-chihbi, K. Dahmani, S. Boukhris, A. Zarrouk, M. EbnTouhami, S-Thiazine as effective inhibitor of mild steel corrosion in HCl solution: synthesis, experimental, theoretical and surface assessment, Colloids Surf. A 613 (2021) 126127.
[36] V. Saraswat, M. Yadav, I.B. Obot, Investigations on eco-friendly corrosion inhibitors for mild steel in acid environment: electrochemical, DFT and Monte Carlo simulation approach, Colloids Surf. A 599 (2020) 124881.
[37] A.Y. Musa, A.A.H. Kadhum, M.S. Takriff, A.R. Daud, S.K. Kamarudin, N. Muhamad, Corrosion inhibitive property of 4-amino-5-phenyl-4H-1,2,4-triazole-3-thiol for mild steel corrosion in 1.0M hydrochloric acid, Corros. Eng. Sci. Technol. 45 (2) (2010) 163–168.
[38] A. Chetouani, B. Hammouti, T. Benhadda, M. Daoudi, Inhibitive action of bipyrazolic type organic compounds towards corrosion of pure iron in acidic media, Appl. Surf. Sci 249 (1-4) (2005) 375–385.
[39] M. Elayyachy, M. Elkodadi, A. Aouniti, A. Ramdani, B. Hammouti, F. Malek, A. Elidrissi, New bipyrazole derivatives as corrosion inhibitors for steel in hydrochloric acid solutions, Mater. Chem. Phys. 93 (2-3) (2005) 281–285.
[40] K. Tebbji, B. Hammouti, H. Oudda, A. Ramdani, M. Benkadour, The inhibitive effect of bipyrazolic derivatives on the corrosion of steel in hydrochloric acid solution, Appl. Surf. Sci 252 (5) (2005) 1378–1385.
[41] K. Cherrak, M. Belghiti, A. Berrissoul, M. El Massaoudi, M. El Faydy, M. Taleb, S. Radi, A. Zarrouk, A. Dafali, Pyrazole carbohydrazide as corrosion inhibitor for mild steel in HCl medium: experimental and theoretical investigations, Surf. Interfaces 20 (2020) 100578.
[42] C. Verma, V.S. Saji, M. Quraishi, E. Ebenso, Pyrazole derivatives as environmental benign acid corrosion inhibitors for mild steel: experimental and computational studies, J. Mol. Liq. 298 (2020) 111943.
[43] F. Boudjellal, H. Ouici, A. Guendouzi, O. Benali, A. Sehmi, Experimental and theoretical approach to the corrosion inhibition of mild steel in acid medium by a newly synthesized pyrazole carbothioamide heterocycle, J. Mol. Struct. 1199 (2020) 127051.
[44] S. El Arrouji, K. Karrouchi, A. Berisha, K.I. Alaoui, I. Warad, Z. Rais, S. Radi, M. Taleb, A. Zarrouk, New pyrazole derivatives as effective corrosion inhibitors on steel-electrolyte interface in 1 M HCl: electrochemical, surface morphological (SEM) and computational analysis, Colloids Surf. A 604 (2020) 125325.
[45] G.H. Sayed, M.E. Azab, K.E. Anwer, M.A. Raouf, N.A. Negm, Pyrazole, pyrazolone and enaminonitrile pyrazole derivatives: synthesis, characterization and potential in corrosion inhibition and antimicrobial applications, J. Mol. Liq. 252 (2018) 329–338.
[46] M. Abdallah, Corrosion behaviour of 304 stainless steel in sulphuric acid solutions and its inhibition by some substituted pyrazolones, Mater. Chem. Phys. 82 (3) (2003) 786–792.
[47] P. Dohare, K.R. Ansari, M.A. Quraishi, I.B. Obot, Pyranpyrazole derivatives as novel corrosion inhibitors for mild steel useful for industrial pickling process: experimental and quantum chemical study, J. Ind. Eng. Chem. 52 (2017) 197–210.
[48] R.A. Hameed, H. Al-Shafey, A.A. Magd, H. Shehata, Pyrazole derivatives as corrosion inhibitor for C-steel in hydrochloric acid medium, J. Mater. Environ. Sci. 3 (2) (2012) 294–305.
[49] P.K. Paul, M. Yadav, I. Obot, Investigation on corrosion protection behavior and adsorption of carbohydrazide-pyrazole compounds on mild steel in 15% HCl solution: electrochemical and computational approach, J. Mol. Liq. 314 (2020) 113513.
[50] X. Li, S. Deng, H. Fu, Triazolyl blue tetrazolium bromide as a novel corrosion inhibitor for steel in HCl and H2SO4 solutions, Corros. Sci. 53 (1) (2011) 302–309.
[51] S. Fatima, R. Sharma, F. Asghar, A. Kamal, A. Badshah, H.B. Kraatz, Study of new amphiphiles based on ferrocene containing thioureas as efficient corrosion inhibitors: gravimetric, electrochemical, SEM and DFT studies, J. Ind. Eng. Chem. 76 (2019) 374–387.
[52] S. Hejazi, S. Mohajernia, M.H. Moayed, A. Davoodi, M. Rahimizadeh, M. Momeni, A. Eslami, A. Shiri, A. Kosari, Electrochemical and quantum chemical study of thiazolo-pyrimidine derivatives as corrosion inhibitors on mild steel in 1 M H2SO4, J. Ind. Eng. Chem. 25 (2015) 112–121.
[53] E.M. Sherif, Electrochemical investigations on the corrosion inhibition of aluminum by 3-amino-1,2,4-triazole-5-thiol in naturally aerated stagnant seawater, J. Ind. Eng. Chem. 19 (6) (2013) 1884–1889.
[54] K. Rasheeda, D. Vijaya, P. Krishnaprasad, S. Samshuddin, Pyrimidine derivatives as potential corrosion inhibitors for steel in acid medium-an overview, Int. J. Corros. Scale Inhib. 7 (1) (2018) 48–61.
[55] Y. Xu, S. Zhang, W. Li, L. Guo, S. Xu, L. Feng, L.H. Madkour, Experimental and theoretical investigations of some pyrazolo-pyrimidine derivatives as corrosion inhibitors on copper in sulfuric acid solution, Appl. Surf. Sci 459 (2018) 612–620.
[56] K.R. Ansari, M.A. Quraishi, Bis-Schiff bases of isatin as new and environmentally benign corrosion inhibitor for mild steel, J. Ind. Eng. Chem. 20 (5) (2014) 2819–2829.
[57] M.A. Hegazy, I. Aiad, 1-Dodecyl-4-(((3-morpholinopropyl)imino)methyl) pyridin-1-ium bromide as a novel corrosion inhibitor for carbon steel during phosphoric acid production, J. Ind. Eng. Chem. 31 (2015) 91–99.
[58] N.A. Wazzan, DFT calculations of thiosemicarbazide, arylisothiocynates, and 1-aryl-2,5-dithiohydrazodicarbonamides as corrosion inhibitors of copper in an aqueous chloride solution, J. Ind. Eng. Chem. 26 (2015) 291–308.
[59] X. He, J. Mao, Q. Ma, Y. Tang, Corrosion inhibition of perimidine derivatives for mild steel in acidic media: electrochemical and computational studies, J. Mol. Liq. 269 (2018) 260–268.
[60] M. Gümüş, N. Gümüş, H.E. Eroğlu, İ. Koca, Design, synthesis and cytotoxic activities of pyrazole-perimidine hybrids, ChemistrySelect 5 (20) (2020) 5916–5921.
[61] C. Verma, L.O. Olasunkanmi, E.E. Ebenso, M.A. Quraishi, I.B. Obot, Adsorption behavior of glucosamine-based, pyrimidine-fused heterocycles as green corrosion inhibitors for mild steel: experimental and theoretical studies, J. Phys. Chem. C 120 (21) (2016) 11598–11611.
[62] C. Verma, L.O. Olasunkanmi, T.W. Quadri, E.-S.M. Sherif, E.E. Ebenso, Gravimetric, electrochemical, surface morphology, DFT, and Monte Carlo simulation studies on three N-substituted 2-aminopyridine derivatives as corrosion inhibitors of mild steel in acidic medium, J. Phys. Chem. C 122 (22) (2018) 11870–11882.
[63] B. Tan, S. Zhang, Y. Qiang, W. Li, H. Li, L. Feng, L. Guo, C. Xu, S. Chen, G. Zhang, Experimental and theoretical studies on the inhibition properties of three diphenyl disulfide derivatives on copper corrosion in acid medium, J. Mol. Liq. 298 (2020) 111975.
[64] M. Lagrenee, B. Mernari, M. Bouanis, M. Traisnel, F. Bentiss, Study of the mechanism and inhibiting efficiency of 3, 5-bis (4-methylthiophenyl)-4H-1, 2, 4-triazole on mild steel corrosion in acidic media, Corros. Sci. 44 (3) (2002) 573–588.
[65] P. Li, J. Lin, K. Tan, J. Lee, Electrochemical impedance and X-ray photoelectron spectroscopic studies of the inhibition of mild steel corrosion in acids by cyclohexylamine, Electrochim. Acta 42 (4) (1997) 605–615.
[66] M. Vaughan, A. Karayan, A. Srivastava, B. Mansoor, J. Seitz, R. Eifler, I. Karaman, H. Castaneda, H. Maier, The effects of severe plastic deformation on the mechanical and corrosion characteristics of a bioresorbable Mg-ZKQX6000 alloy, Mater. Sci. Eng. 115 (2020) 111130.
[67] Z. Salarvand, M. Amirnasr, M. Talebian, K. Raeissi, S. Meghdadi, Enhanced corrosion resistance of mild steel in 1 M HCl solution by trace amount of 2-phenyl-benzothiazole derivatives: experimental, quantum chemical calculations and molecular dynamics (MD) simulation studies, Corros. Sci. 114 (2017) 133–145.
[68] P. Mourya, S. Banerjee, M. Singh, Corrosion inhibition of mild steel in acidic solution by *Tagetes erecta* (Marigold flower) extract as a green inhibitor, Corros. Sci. 85 (2014) 352–363.
[69] Z. Mahidashti, T. Shahrabi, B. Ramezanzadeh, A new strategy for improvement of the corrosion resistance of a green cerium conversion coating through thermal treatment procedure before and after application of epoxy coating, Appl. Surf. Sci. 390 (2016) 623–632.
[70] A. Singh, K.R. Ansari, M.A. Quraishi, Y. Lin, Investigation of corrosion inhibitors adsorption on metals using density functional theory and molecular dynamics simulation, Corrosion Inhibitors, IntechOpen2019.
[71] D.K. Verma, Density functional theory (DFT) as a powerful tool for designing corrosion inhibitors in aqueous phase, in: A. Ali (Ed.), Advanced Engineering Testing, IntechOpen, London, 2018, p. 87.
[72] I. Obot, D. Macdonald, Z. Gasem, Density functional theory (DFT) as a powerful tool for designing new organic corrosion inhibitors. Part 1: an overview, Corros. Sci. 99 (2015) 1–30.
[73] M. Chafiq, A. Chaouiki, H. Lgaz, R. Salghi, S.L. Gaonkar, K.S. Bhat, R. Marzouki, I.H. Ali, M.I. Khan, H. Shimizu, Synthesis and corrosion inhibition evaluation of a new Schiff base hydrazone for mild steel corrosion in HCl medium: electrochemical, DFT, and molecular dynamics simulations studies, J. Adhes. Sci. Technol. 34 (12) (2020) 1283–1314.
[74] M.J. Frisch, G. Trucks, H. Schlegel, G. Scuseria, M. Robb, J. Cheeseman, G. Scalmani, V. Barone, B. Mennucci, G. Petersson, Gaussian 09, Revision D. 01, Gaussian, Inc., Wallingford, CT, 2009.
[75] R. Dennington, T. Keith, J. Millam, GaussView, Version 5, Semichem Inc., Shawnee Mission, KS, 2009.
[76] A.S. Lileev, V.L. Dar'ya, A.K. Lyashchenko, Dielectric properties of aqueous hydrochloric acid solutions, Mendeleev Commun. 17 (6) (2007) 364–365.
[77] J. Tomasi, B. Mennucci, R. Cammi, Quantum mechanical continuum solvation models, Chemical reviews 105 (8) (2005) 2999–3094.
[78] E. Cances, B. Mennucci, J. Tomasi, A new integral equation formalism for the polarizable continuum model: theoretical background and applications to isotropic and anisotropic dielectrics, J. Chem. Phys. 107 (8) (1997) 3032–3041.
[79] B. Mennucci, J. Tomasi, Continuum solvation models: a new approach to the problem of solute's charge distribution and cavity boundaries, J. Chem. Phys. 106 (12) (1997) 5151–5158.

[80] B. Mennucci, E. Cances, J. Tomasi, Evaluation of solvent effects in isotropic and anisotropic dielectrics and in ionic solutions with a unified integral equation method: theoretical bases, computational implementation, and numerical applications, J. Phys. Chem. B 101 (49) (1997) 10506–10517.
[81] J. Tomasi, B. Mennucci, E. Cancès, The IEF version of the PCM solvation method: an overview of a new method addressed to study molecular solutes at the QM ab initio level, J. Mol. Struct. 464 (1-3) (1999) 211–226.
[82] V. Sastri, J. Perumareddi, Molecular orbital theoretical studies of some organic corrosion inhibitors, Corrosion 53 (08) (1997) NACE–97080617.
[83] N.V. Bondarev, K.P. Katin, V.B. Merinov, A.I. Kochaev, S. Kaya, M.M. Maslov, Probing of neural networks as a bridge from ab initio relevant characteristics to differential scanning calorimetry measurements of high-energy compounds, Phys. Status Solidi (RRL)–Rapid Res. Lett. 16 (3) (2022) 2100191.
[84] T. Koopmans, Über die Zuordnung von Wellenfunktionen und Eigenwerten zu den einzelnen Elektronen eines Atoms, Physica 1 (1-6) (1934) 104–113.
[85] R.G. Pearson, Absolute electronegativity and hardness: application to inorganic chemistry, Inorganic 27 (4) (1988) 734–740.
[86] R.M. Kubba, A.S. Alag, Experimental and theoretical evaluation of new quinazolinone derivative as organic corrosion inhibitor for carbon steel in 1M HCl solution, Int. J. Sci. Res. 6 (6) (2017) 1832–1843.
[87] C. Verma, J. Haque, E.E. Ebenso, M. Quraishi, Melamine derivatives as effective corrosion inhibitors for mild steel in acidic solution: chemical, electrochemical, surface and DFT studies, Results Phys. 9 (2018) 100–112.
[88] C. Verma, M. Quraishi, A. Singh, 5-Substituted 1H-tetrazoles as effective corrosion inhibitors for mild steel in 1 M hydrochloric acid, J. Taibah. Univ. Sci. 10 (5) (2016) 718–733.
[89] C. Verma, M.A. Quraishi, K. Kluza, M. Makowska-Janusik, L.O. Olasunkanmi, E.E. Ebenso, Corrosion inhibition of mild steel in 1M HCl by D-glucose derivatives of dihydropyrido [2, 3-d: 6, 5-d′] dipyrimidine-2, 4, 6, 8 (1H, 3H, 5H, 7H)-tetraone, Sci. Rep. 7 (1) (2017) 1–17.
[90] A. Dehghani, G. Bahlakeh, B. Ramezanzadeh, M. Ramezanzadeh, Potential of Borage flower aqueous extract as an environmentally sustainable corrosion inhibitor for acid corrosion of mild steel: electrochemical and theoretical studies, J. Mol. Liq. 277 (2019) 895–911.
[91] D. Kumar, V. Jain, B. Rai, Capturing the synergistic effects between corrosion inhibitor molecules using density functional theory and ReaxFF simulations-a case for benzyl azide and butyn-1-ol on Cu surface, Corros. Sci. 195 (2022) 109960.
[92] T.L.M. Pham, T.K. Phung, H.V. Thang, DFT insights into the adsorption mechanism of five-membered aromatic heterocycles containing N, O, or S on Fe (110) surface, Appl. Surf. Sci. (2022) 152524.
[93] E. Ebenso, Synergistic effect of halide ions on the corrosion inhibition of aluminium in H2SO4 using 2-acetylphenothiazine, Mater. Chem. Phys. 79 (1) (2003) 58–70.
[94] E. Berdimurodov, A. Kholikov, K. Akbarov, L. Guo, S. Kaya, K.P. Katin, D.K. Verma, M. Rbaa, O. Dagdag, R. Haldhar, Novel gossypol–indole modification as a green corrosion inhibitor for low–carbon steel in aggressive alkaline–saline solution, Colloids Surf. A (2022) 128207.
[95] J.D. Smith, The Use of Histidine-Containing Polyamino Acids as Corrosion Inhibitors and Antiscalants, University of South Alabama, 1995.
[96] R. Sanderson, Electronegativities in inorganic chemistry:(II), J. Chem. Educ. 31 (1) (1954) 2.
[97] R.T. Sanderson, Electronegativity and bond energy, J. Am. Chem. Soc. 105 (8) (1983) 2259–2261.
[98] A.A. Abdulridha, M.A.A.H. Allah, S.Q. Makki, Y. Sert, H.E. Salman, A.A. Balakit, Corrosion inhibition of carbon steel in 1 M H2SO4 using new Azo Schiff compound: electrochemical, gravimetric, adsorption, surface and DFT studies, J. Mol. Liq. 315 (2020) 113690.
[99] M. Dehdab, M. Shahraki, S.M. Habibi-Khorassani, Theoretical study of inhibition efficiencies of some amino acids on corrosion of carbon steel in acidic media: green corrosion inhibitors, J. Amino Acids 48 (1) (2016) 291–306.
[100] S.K. Saha, P. Banerjee, Introduction of newly synthesized Schiff base molecules as efficient corrosion inhibitors for mild steel in 1 M HCl medium: an experimental, density functional theory and molecular dynamics simulation study, Mater. Chem. Front. 2 (9) (2018) 1674–1691.
[101] M. Bedair, S. Soliman, M. Hegazy, I. Obot, A. Ahmed, Empirical and theoretical investigations on the corrosion inhibition characteristics of mild steel by three new Schiff base derivatives, J. Adhes. Sci. Technol. 33 (11) (2019) 1139–1168.
[102] G. Cui, J. Guo, Y. Zhang, Q. Zhao, S. Fu, T. Han, S. Zhang, Y. Wu, Chitosan oligosaccharide derivatives as green corrosion inhibitors for P110 steel in a carbon-dioxide-saturated chloride solution, Carbohydr. Polym. 203 (2019) 386–395.
[103] O. Dagdag, A. El Harfi, M. El Gouri, Z. Safi, R.T. Jalgham, N. Wazzan, C. Verma, E. Ebenso, U.P. Kumar, Anticorrosive properties of hexa (3-methoxy propan-1, 2-diol) cyclotri-phosphazene compound for carbon steel in 3% NaCl medium: gravimetric, electrochemical, DFT and Monte Carlo simulation studies, Heliyon 5 (3) (2019) e01340.
[104] T. Verbiest, S. Houbrechts, M. Kauranen, K. Clays, A. Persoons, Second-order nonlinear optical materials: recent advances in chromophore design, J. Mater. Chem. 7 (11) (1997) 2175–2189.
[105] J.J. Wolff, R. Wortmann, Organic materials for second-order non-linear optics, in: Advances in Physical Organic Chemistry, Elsevier, 1999, pp. 121–217.